Front. Earth Sci. 2018, 12(4): 846–861
https://doi.org/10.1007/s11707-017-0643-2

RESEARCH ARTICLE

Evaluation of extreme precipitation based on satellite retrievals over China

Xuerongzi HUANG[1], Dashan WANG[3], Yu LIU[1], Zhizhou FENG[1], Dagang WANG (✉)[1,2,3]

1 Department of Water Resources and Environment, Sun Yat-sen University, Guangzhou 510275, China
2 Key Laboratory of Water Cycle and Water Security in Southern China of Guangdong High Education Institute, Sun Yat-sen University, Guangzhou 510275, China
3 Center of Integrated Geographic Information Analysis, School of Geography and Planning, Sun Yat-sen University, Guangzhou 510275, China

Abstract The objective of this study is to evaluate satellite precipitation extremes of the Tropical Rainfall Measuring Mission (TRMM) 3B42 Version 7 product over China during the period of 2009–2013. Eight extreme indices are used to characterize precipitation extremes: monthly maximum 1-day precipitation (RX1day), monthly maximum consecutive 2-day precipitation (RX2day), monthly maximum 5-day consecutive precipitation (RX5day), simple daily intensity index (SDII), annual total precipitation amount for the wet days (PRCPTOT), annual wet days (R1), consecutive dry days (CDD), and consecutive wet days (CWD). The precipitation amount for indices RX1day, RX2day, RX5day, and PRCPTOT is well captured by TRMM 3B42-V7, as verified by lower mean relative bias and normalized root mean square error and the high spatial correlation coefficient. In contrast, the performance of TRMM 3B42-V7 in depicting the indices on intensity and duration (i.e., SDII, R1, CDD, and CWD) is not as good as its performance in depicting the precipitation amount indices. TRMM 3B42-V7 can reproduce extreme indices better in eastern China than in western China, and better in summer than in winter. Probability density function is also calculated better for RX1day, RX2day, RX5day, and PRCPTOT than for SDII, R1, CDD, and CWD. Investigation on the monthly time series of RX1day, RX2day, and RX5day at different spatial scales indicates that TRMM 3B42-V7 performs better at the large spatial scale than at the grid cell scale. Caution should be observed when the satellite-based extreme indices are used.

Keywords satellite, extreme precipitation, TRMM, China

Received October 17, 2015; accepted January 24, 2017

E-mail: wangdag@mail.sysu.edu.cn

1 Introduction

It is widely recognized that extreme climate events have occurred more frequently under global climate change and intensified anthropogenic activities. For example, Alexander et al. (2013) analyzed the long-term records of daily temperature and precipitation over the globe, and found that a warmer and wetter trend is significant over most land areas throughout the twentieth century. This trend is verified by several regional observation-based studies (Thibeault and Seth, 2014). Moreover, the climate projections indicate that frequency of extreme climate events would increase in the future (Monier and Gao, 2014). Extreme climate events often pose a negative effect on human society and natural ecosystems. From 1972 to 2012, 1.94 million deaths and US$2.4 trillion in economic losses have occurred due to extreme climate events throughout the world (WMO, 2014). Globally, approximately 40 million people in port cities are exposed to more 100-year floods due to sea level rise and storm surge (Hanson et al., 2011). The ecosystem is also significantly affected by extreme events. Plant growth and function are changed by heat waves and drought, which affect the biomass yield (De Boeck et al., 2011). The forest ecosystem would be exposed to higher risk due to the increased mortality rate under extreme climatic conditions (Allen et al., 2010).

Temperature and precipitation are two variables that researchers are mainly concerned with when examining extreme climates. Compared with the former, the latter shows more complex spatiotemporal characteristics. The change in precipitation extremes greatly varies with season and region (Moberg and Jones, 2005; You et al., 2011; Alexander et al., 2013). Worldwide, the precipitation extreme indices for June-July-August do not significantly increase over most land areas, whereas an increase in

precipitation extreme occurs in more areas for other seasons (Alexander et al., 2013). The precipitation extreme indices do not show a significant increasing trend except for heavy precipitation days during 1961–2003 over China (You et al., 2011). In contrast, over Western Europe, a significant increasing trend in precipitation extreme was dominant during the twentieth century in most areas (Moberg and Jones, 2005). It is therefore important to evaluate precipitation extreme regionally and seasonally.

Historical precipitation extreme evaluation is primarily based on gauge observations (Alexander et al., 2013; Westra et al., 2013). Alexander et al. combined station records from the Global Climate Observing System surface network, European Climate Assessment, and the daily Global Historical Climatology Network for global climate extreme analysis (Peterson et al., 1997; Klein Tank et al., 2002; Menne et al., 2012; Alexander et al., 2013). Westra et al. (2013) used precipitation observations from 11,391 stations over the globe in studying the change in precipitation extreme. Precipitation records from stations are believed to be the most reliable estimates of precipitation extreme. However, extensive effort is needed to conduct careful data quality control and ensure homogeneity of data for large regions. Moreover, the station density greatly varies with region, and missing data often occurs, which results in an inadequate temporal sampling and spatial coverage.

Compared with *in situ* data, the precipitation products derived from satellite-based observations provide a wider coverage, which is particularly important for developing countries. For instance, precipitation derived from geostationary satellite infrared (IR) brightness temperature covers most of the globe with high temporal and spatial resolution. In contrast to IR, precipitation derived from passive microwave (PMW) sensors has limitations in temporal and spatial sampling due to low orbit platforms. However, PMW retrievals are believed to be more reliable than IR observations at finer spatial resolutions as it responds to hydrometeor particles instead of the cloud-top features IR uses. To take advantage of both wavelengths, researchers have developed algorithms that combine products from all available sensors. The resulting products are verified to be more accurate at high spatial and temporal resolutions compared with retrievals from a single sensor (Michaelides et al., 2009).

The Climate Prediction Center morphing technique (CMORPH) (Joyce et al., 2004) and the Tropical Rainfall Measuring Mission (TRMM) multi-satellite precipitation analysis (TMPA) (Huffman et al., 2007), which are two examples of such products during the TRMM-era. The core observatory of the Global Precipitation Measurement (GPM) was successfully deployed on February 28, 2014 (Hou et al., 2014). The GPM is regarded as an extension of the TRMM satellite, making a transition of precipitation observation from the TRMM-era to the GPM-era. These satellite-based precipitation products are widely used in climate model validation (Ebert et al., 2007), hydrological prediction (Su et al., 2008), and flood and drought monitoring (Asante et al., 2007; Rhee et al., 2010).

In spite of the usefulness of satellite-based products, the rainfall retrieval uncertainty is large, and its magnitude varies with region (Tian et al., 2009). It is therefore important to evaluate the performance of satellite-based products for a specific region. Research toward this direction includes the validation work conducted in South America (Su et al., 2008), North America (Tian et al., 2009), Asia (Shen et al., 2010b), Africa (Romilly and Gebremichael, 2011), Europe (Kidd et al., 2012), and Oceania (Chen et al., 2013c).

Although evaluations of satellite precipitation against gauge observations have been conducted extensively, only a few studies have particularly focused on extreme precipitation (AghaKouchak et al., 2011; Nastos et al., 2013; Lockhoff et al., 2014). As the effect of extreme precipitation is substantial to human society and natural ecosystems, the object of this study is to evaluate a satellite product in terms of characterizing extreme precipitation over China. This paper is organized as follows: Section 2 describes the satellite-based data to be evaluated and the gauge data. Methods are introduced in Section 3. Results are presented in Section 4. Section 5 summarizes this study.

2 Data

2.1 Satellite-based data

The TMPA 3B42 research product, which is a combination of PMW and IR data and further adjusted by gauge observations, was chosen to evaluate the performance of satellite retrievals in capturing precipitation extremes. As described by Huffman et al. (2007), to produce Version 6 of the 3B42 research product, the combined PWM images are derived from the Microwave Imager on TRMM (TMI), Special Sensor Microwave Imager (SSM/I) on the Defense Meteorological Satellite Program satellites, Advanced Microwave Scanning Radiometer-Earth Observing System (AMSR-E) on Aqua, and the Advanced Microwave Sounding Unit-B (AMSU-B) on the National Oceanic and Atmospheric Administration (NOAA) satellite series. The IR-based scans, which are collected by the international constellation of geosynchronous earth orbit satellites, are used to fill the spatial gap the PWM-based retrievals do not cover. In addition, the Global Precipitation Climatology Project monthly data are incorporated into the combined PMW–IR data to reduce bias. Shen et al. (2010b) compared six satellite-based precipitation products over China and found that TRMM 3B42 Version 6 has the smallest bias because of gauge adjustments.

In 2012, the TMPA algorithm was upgraded from version 6 to version 7. The differences between version 6

and version 7 are as follows (Huffman and Bolvin, 2013; Yong et al., 2015): 1) additional microwave products, i.e., NOAA Microwave Humidity Sounder (MHS) and Special Sensor Microwave Imager/Sounder (SSMIS); 2) a new IR dataset, i.e., the National Climatic Data Center (NCDC) GridSat-B1; 3) uniform processing of input data (AMSU, MHS, TMI, AMSR-E, SSM/I, etc.); 4) use of a single and uniformly processed gauge analysis; 5) a latitude band calibration scheme for all satellites; and 6) additional fields in the data files (sensor-specific source and overpass time).

In the past two years, quite a number of studies compared version 6 and version 7 of TRMM 3B42 estimates. Chen et al. (2013a,b) systematically studied the spatiotemporal error characteristics of the version 6 and 7 of TMPA products over continental US and mainland China, respectively, and found that 3B42-V7 better agree with observations and reduces the data bias over most regions. Yong et al. (2014) demonstrated that 3B42-V7 is superior to its previous version over two basins in China through a 7-year evaluation. In other studies, researchers found 3B42-V7 can largely reduce the underestimation that exists in 3B42-V6 over the Southern US (Qiao et al., 2014), and has reduced the system error for heavy rainfall (Liu, 2015). Generally, version 7 of TRMM 3B42 shows overall improvement over a variety of areas compared with version 6 (Chen et al., 2013a,b; Yong et al., 2014; Zulkafli et al., 2014).

GPM extends the frequency of precipitation radar and microwave imager, and provides precipitation estimates using the Day-1 Integrated Multi-satellite algorithm for GPM (IMERG) (Huffman et al., 2014). Compared with the previous satellite-based precipitation products, IMERG has finer resolution (0.1° and half-hourly) and world-wide spatial coverage, and is expected to bring new insights into the light rainfall, as well as solid precipitation. Recently, some efforts have been made to validate the GPM IMERG estimates. Tang et al. (2016) compared the performance of IMERG and 3B42-V7 over mainland China, and found that IMERG shows better performance at multiple time-scales and over different regions, although the limitation still exists in capturing the precipitation over high-latitude regions and dry areas. An assessment work of the IMERG estimate for detecting heavy rainfall over India was presented by Prakash et al. (2016). They found that IMERG greatly improves data quality over 3B42-V7 during the monsoon season, while it has similar performances with 3B42-V7 in terms of the volume of hit, missed, and false precipitation. Li et al. (2017) investigated the utility of IMERG estimate via data validation and hydrological modeling approaches over the Ganjiang River basin in China. The results highlight the potential usage of IMERG on account of its coverage and continuity, although the gap between the performance of IMERG and that of radar and gauge precipitation data is noteworthy. Since the IMERG precipitation estimate only covered a period from mid-March, 2014 to date, we used precipitation estimates from TRMM 3B42 Version 7 (hereafter TRMM 3B42-V7) in this study to provide long-term validation work.

2.2 Reference data

China Daily Precipitation Analysis Products (CPAP) Version 1.0, developed by the National Meteorological Information Center of the China Meteorological Administration (Shen et al., 2010a; http://cdc.nmic.cn/home.do), was used as the ground truth for evaluation. The process to produce CAPA data is as follows: 1) the daily precipitation observations are obtained from more than 2400 gauge measurements; 2) the high frequency noise of the observations is excluded by the Fourier transform; 3) the algorithm of Shepard is employed to interpolate the gauge data to daily climatology in 0.05°×0.05° grids; 4) the daily climatology is adjusted by the PRISM (Parameter-elevation Regressions on Independent Slopes Model) to take the terrain effect into account; 5) the optimal interpolation (OI) technique which can reduce the analysis error from the spatial discontinuity of precipitation is used to obtained the daily precipitation ratio fields in 0.05°×0.05° grids; 6) the final daily precipitation is calculated by multiplying the daily climatology with the daily precipitation ratio, and then resampling the data into 0.25°×0.25° grids.

An evaluation experiment at a gauge in southeastern China indicated that the relative bias is 3.21% when compared with independent gauge observations (Shen et al., 2010a). CPAP has been used to evaluate satellite retrievals throughout China (Chen et al., 2013c). While the spatial resolution is the same for the two products (0.25°×0.25°), the temporal resolution differs (3-hourly for TRMM 3B42-V7, and daily for CPAP). We aggregated TRMM 3B42-V7 from 3-hourly to daily to match the temporal resolution of CPAP. 3B42-V7 covers a period from 1998 to date, and CPAP is freely available since 1961. In this study, we choose a 5-year period from 2009 to 2013 to evaluate the ability of TRMM 3B42-V7 in characterizing extreme precipitation throughout China, the South China Sea Islands and Taiwan Island are important parts of China but they were not included in the evaluation in this study. In addition, the zone beyond 50°N was not included in the evaluation, as TRMM 3B42 covers 50°S to 50°N.

3 Methods

3.1 Precipitation extreme indices

The joint World Meteorological Organization Commission for Climatology (CCl)/World Climate Research Programme (WCRP) project on Climate Variability and Predictability (CLIVAR) Expert Team on Climate Change Detection and Indices (ETCCDI) proposed 10 precipita-

tion extreme indices based on daily precipitation, including monthly maximum 1-day precipitation amount (RX1day), monthly maximum consecutive 5-day precipitation amount (RX5day), annual total precipitation from wet days (PRCPTOT), simple daily intensity index (SDII), consecutive dry days (CDD), consecutive wet days (CWD), annual count when precipitation $\geqslant$ 10 mm (R10), annual count when precipitation $\geqslant$20 mm (R20), annual total precipitation from days $\geqslant 95^{\text{th}}$ percentile (R95p), and annual total precipitation from days $\geqslant$ 99^{th} percentile (R99p). Wet and dry days are distinguished by 1 mm.

As the daily precipitation over a large portion of western China seldom exceeds 10 mm, R10 and R20 were not included in the evaluation. In addition, R95p and R99p were excluded because the long-term 0.25°×0.25° daily precipitation data were not available. SDII was calculated as the ratio of PRCPTOT to annual count of wet days (R1). To assess the relative contribution of PRCPTOT and R1 to SDII, R1 was chosen to be one of the indices. Monthly maximum consecutive 2-day precipitation amount (RX2day) was added in the evaluation to investigate the effect of temporal scale on the performance of satellite precipitation. Therefore, the eight indices used in this study are RX1day, RX2day, RX5day, SDII, PRCPTOT, R1, CDD, and CWD.

3.2 Statistics

To assess the quality of satellite precipitation at the grid cell scale, the relative bias (RB) was used and defined as follows:

$$RB_i = 100\% \times \frac{PS_i - PG_i}{PG_i}, i = 1,2,...,N, \quad (1)$$

where PS is the satellite precipitation, PG is the CPAP precipitation, i is the grid cell number, and N is the total number of grid cells.

We divided China into eastern and western China, with 105°E as the boundary. Following Zhao and Yatagai (2014), three statistics, mean relative bias (MRB), normalized root mean square error (NRMSE), and correlation coefficient (CC), were used to evaluate the performance of satellite precipitation at the regional scale (i.e., China as a whole, eastern China, and western China). It is noted that both RB and MRB are used to indicate the accumulative retrieval bias of estimates. However, MRB is different from RB in that it is used to evaluate the overall bias of estimates by spatially averaging RB over different study areas.

The statistics are calculated as follows:

$$\text{MRB} = 100\% \times \frac{1}{N}\sum_{i=1}^{i=N}\frac{PS_i - PG_i}{PG_i}, \quad (2)$$

$$\text{NRMSE} = \frac{\sqrt{\frac{1}{N}\sum_{i=1}^{N}(PS_i - PG_i)^2}}{\frac{1}{N}\sum_{i=1}^{N}PG_i}, \quad (3)$$

$$\text{CC} = \frac{\sum_{i=1}^{i=N}\left(PS_i - \overline{PS}\right)\left(PG_i - \overline{PG}\right)}{\sqrt{\sum_{i=1}^{i=N}\left(PS_i - \overline{PS}\right)^2}\sqrt{\sum_{i=1}^{i=N}\left(PG_i - \overline{PG}\right)^2}}. \quad (4)$$

To investigate the performance of TRMM 3B42-V7 in capturing precipitation extreme with different levels, we compared the empirical probability density functions (PDFs) for satellite precipitation and CPAP precipitation. Additionally, the monthly time series of RX1day, RX2day, and RX5day produced by TRMM 3B42-V7 was evaluated against CPAP. The CC between the time series of these two products was calculated in the same way as Eq. (4) except for the representation of i and N. For the CC of the time series between TRMM 3B42-V7 and CPAP, i and N represent month number and the total number of months, respectively.

4 Results

We take the 5-year (2009−2013) averages of extreme indices for evaluation unless the temporal scales of indices are specified in this study, since the relative error of TRMM 3B42-V7 in annual precipitation for each individual year is similar to the 5-year averaged relative error in both spatial pattern and magnitude (not shown).

4.1 Spatial pattern and statistics

The performance of TRMM 3B42-V7 in depicting RX1day, RX2day, and RX5day is presented in Tables 1, 2, and 3. TRMM 3B42-V7 generally overestimates the maximum precipitation amount when China is taken as a whole, and this overestimation decreases with the increase of the temporal scale (i.e., from 1 day to 5 days), as shown in Table 1. The overestimation is more evident over eastern China. However, underestimation usually exists over western China except for winter. When all grid cells over China are considered, MRB for RX1day is substantially larger than that for RX5day (10.28% versus 3.19%), whereas NRMSE and CC remain similar for all three indices. The NRMSE (CC) values are 0.35 (0.92), 0.31 (0.93), and 0.30 (0.94) for RX1day, RX2day, and RX5day, respectively. The performance of TRMM 3B42-V7 in estimating the maximum precipitation amounts varies with region, and season. Regionally, TRMM 3B42-V7 is better over eastern China based on NRMSE and CC, while it is

Table 1 Relative bias (MRB) of TRMM 3B42-V7 against CPAP for different regions and different seasons. Western (eastern) China here is defined as west (east) of 105°E

Index	Region	Annual	Spring	Summer	Autumn	Winter
RX1day	China	10.28	10.37	1.53	4.10	43.72
	Eastern China	15.21	23.59	5.83	16.32	56.97
	Western China	−0.08	−19.99	−8.23	−22.37	12.67
RX2day	China	5.25	4.21	−1.59	−0.49	34.85
	Eastern China	9.82	17.29	2.43	11.07	47.77
	Western China	−4.30	−24.81	−10.47	−24.78	3.71
RX5day	China	3.19	3.20	−1.86	−2.10	26.61
	Eastern China	7.17	13.82	2.34	8.49	37.32
	Western China	−4.81	−21.27	−10.42	−22.83	−1.68

Table 2 Normalized root mean square error (NRMSE) of TRMM 3B42-V7 against CPAP for different regions and different seasons. Western (eastern) China here is defined as west (east) of 105°E

Index	Region	Annual	Spring	Summer	Autumn	Winter
RX1day	China	0.35	0.54	0.34	0.64	1.22
	Eastern China	0.25	0.42	0.21	0.32	1.08
	Western China	0.56	0.81	0.6	1.13	1.31
RX2day	China	0.32	0.5	0.32	0.55	1.1
	Eastern China	0.2	0.36	0.19	0.27	0.95
	Western China	0.56	0.83	0.59	0.97	1.26
RX5day	China	0.3	0.45	0.32	0.49	0.93
	Eastern China	0.16	0.28	0.17	0.23	0.77
	Western China	0.57	0.82	0.58	0.84	1.18

Table 3 Correlation coefficient (CC) of TRMM 3B42-V7 against CPAP for different regions and different seasons. Western (eastern) China here is defined as west (east) of 105°E

Index	Region	Annual	Spring	Summer	Autumn	Winter
RX1day	China	0.92	0.88	0.87	0.72	0.85
	Eastern China	0.95	0.95	0.88	0.91	0.91
	Western China	0.82	0.74	0.73	0.47	0.72
RX2day	China	0.93	0.88	0.89	0.79	0.87
	Eastern China	0.97	0.96	0.91	0.94	0.93
	Western China	0.84	0.77	0.78	0.56	0.73
RX5day	China	0.94	0.92	0.90	0.84	0.90
	Eastern China	0.97	0.98	0.93	0.95	0.94
	Western China	0.86	0.81	0.82	0.67	0.73

usually the best over China as a whole based on MRB because of the offset between positive and negative biases over the large area. However, the winter MRB over western China is the smallest among the three areas. For example, the winter MRB for RX5day is −1.68 over western China, whereas the same statistic is 37.32 over eastern China. Seasonally, TRMM 3B42-V7 is usually the best in summer but the worst in autumn and winter. In summary, TRMM 3B42-V7 performs best in producing RX5day over eastern China in summer, as verified by small values of MRB (2.34%) and NRMSE (0.17), and large values of CC (0.93).

The performance of TRMM 3B42-V7 in simulating SDII is similar to that in simulating the maximum precipitation amount, with a negative bias in western China and a positive bias in eastern China, as shown in Table 4. In contrast, the positive (negative) bias for R1 is found in western (eastern) China. Compared with SDII and R1, PRCPTOT is well simulated by TRMM 3B42-V7 even though a large bias still exists in western China. The values of MRB and NRMSE for PRCPTOT over China are smaller than the values for SDII and R1, and the CC value for PRCPTOT over China is much larger than that for SDII and R1. A considerable positive bias evidently occurs for SDII (16.30%) over eastern China, which mainly results from the large negative bias for R1 (−11.18%). The negative bias for SDII (−14.23%) over western China is attributed to both the negative bias for PRCPTOT (−5.88%) and positive bias for R1 (3.61%). NRMSE and CC values are different for different seasons and are usually better for eastern China than for western China. For example, NRMSE for SDII over eastern China is 0.26, which is much smaller than that over western China (0.42).

The performance of TRMM 3B42-V7 in simulating SDII is similar to that in simulating the maximum precipitation amount, with a negative bias in western China and a positive bias in eastern China, as shown in Table 4. In contrast, the positive (negative) bias for R1 is found in western (eastern) China. Compared with SDII and R1, PRCPTOT is well simulated by TRMM 3B42-V7 even though a large bias still exists in western China. The values of MRB and NRMSE for PRCPTOT over China are smaller than the values for SDII and R1, and the CC value for PRCPTOT over China is much larger than that for SDII and R1. A considerable positive bias evidently occurs for SDII (16.30%) over eastern China, which mainly results from the large negative bias for R1 (−11.18%). The negative bias for SDII (−14.23%) over western China is attributed to both the negative bias for PRCPTOT (−5.88%) and positive bias for R1 (3.61%). NRMSE and CC values are different for different seasons and are usually better for eastern China than for western China. For example, NRMSE for SDII over eastern China is 0.26, which is much smaller than that over western China (0.42).

Generally, TRMM 3B42-V7 does not perform well in capturing CDD and CWD, as reflected by the spatial patterns of CDD and CWD derived from TRMM 3B42-V7 and CPAP (now shown) and statistics in Table 4. The positive and negative biases for CDD are mixed, and the negative bias for CWD dominates over China (now shown). As shown in Table 4, NRMSE is also considerably large for both CDD and CWD, and the CC values are much smaller than those for other indices. TRMM 3B42-V7 performs better over eastern China than over western China based on the NRMSE value, and is indeed similar based on the CC value for both CDD and CWD.

4.2 PDF

Frequency is analyzed for the eight indices. Figure 1 shows the PDFs of RX1day, RX2day, and RX5day over the whole of China. Generally, TRMM 3B42-V7 reasonably captures the frequencies of these indices over China, and the TRMM-based frequencies become closer to the CPAP-based frequencies as the temporal scales of the indices increase. However, a discrepancy between CPAP and TRMM 3B42-V7 exists. TRMM 3B42-V7 tends to overestimate the relative frequency when the extreme precipitation amount is lower than ~10 mm in all seasons except winter. Underestimation in relative frequency occurs for the extreme precipitation amount of ~10–40 mm. When the extreme precipitation amount is very large ($>$ ~30 mm for RX1day, $>$ ~40 for RX2day, and $>$ ~50 for RX5day), TRMM 3B42-V7 overestimates the relative frequency.

TRMM 3B42-V7 performs better in reproducing the relative frequency of RX1day, RX2day, and RX5day over eastern China (Fig. 2) than over China's entirety (Fig. 1). TRMM 3B42-V7 underestimates frequency for precipitation under ~40 mm and overestimation for precipitation above ~40 mm. The RX5day frequency produced by TRMM 3B42-V7 agrees better with that derived from

Table 4 The mean of PRCPTOT, R1, SDII, CDD and CWD based on gauge observations, and root mean square error (RMSE), relative bias (RB), and correlation coefficient (CC) of TRMM 3B42 against CPAP for different regions

Statistics	Region	SDII	PRCPTOT	R1	CDD	CWD
MRB/%	China	3.72	−0.2	−4.83	−0.32	−11.77
	Eastern China	16.30	2.75	−11.18	7.92	−13.07
	Western China	−14.23	−5.88	3.61	−5.05	−10.54
NRMSE	China	0.33	0.31	0.32	0.34	0.56
	Eastern China	0.26	0.13	0.25	0.27	0.43
	Western China	0.42	0.60	0.41	0.35	0.66
CC	China	0.82	0.94	0.84	0.68	0.57
	Eastern China	0.88	0.98	0.84	0.65	0.52
	Western China	0.81	0.88	0.84	0.61	0.58

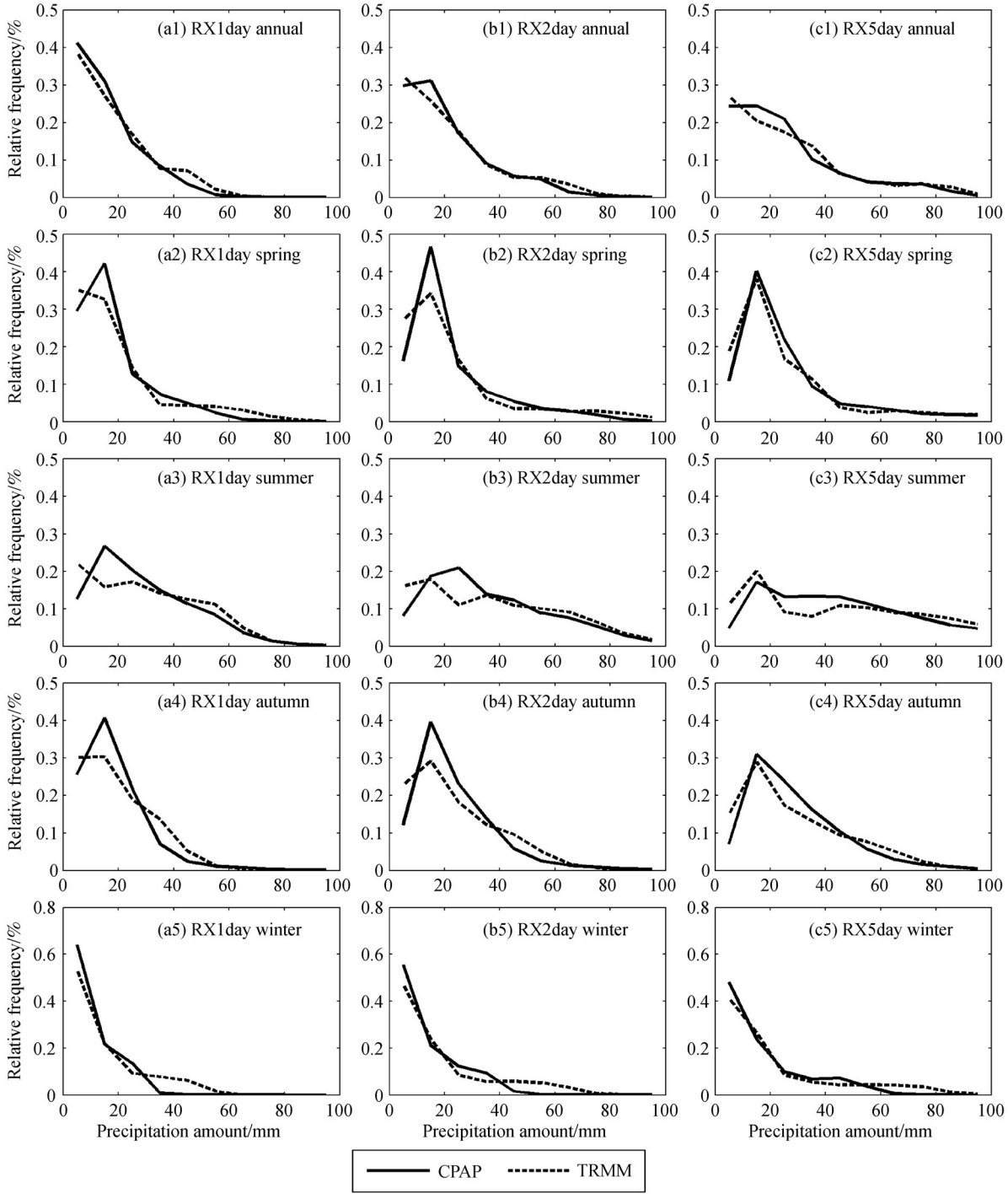

Fig. 1 The relative frequency of (a) RX1day, (b) RX2day, and (c) RX5day derived from CPAP and TRMM 3B42-V7 1) annually, and in four seasons: 2) spring, 3) summer, 4) autumn, 5) winter over China.

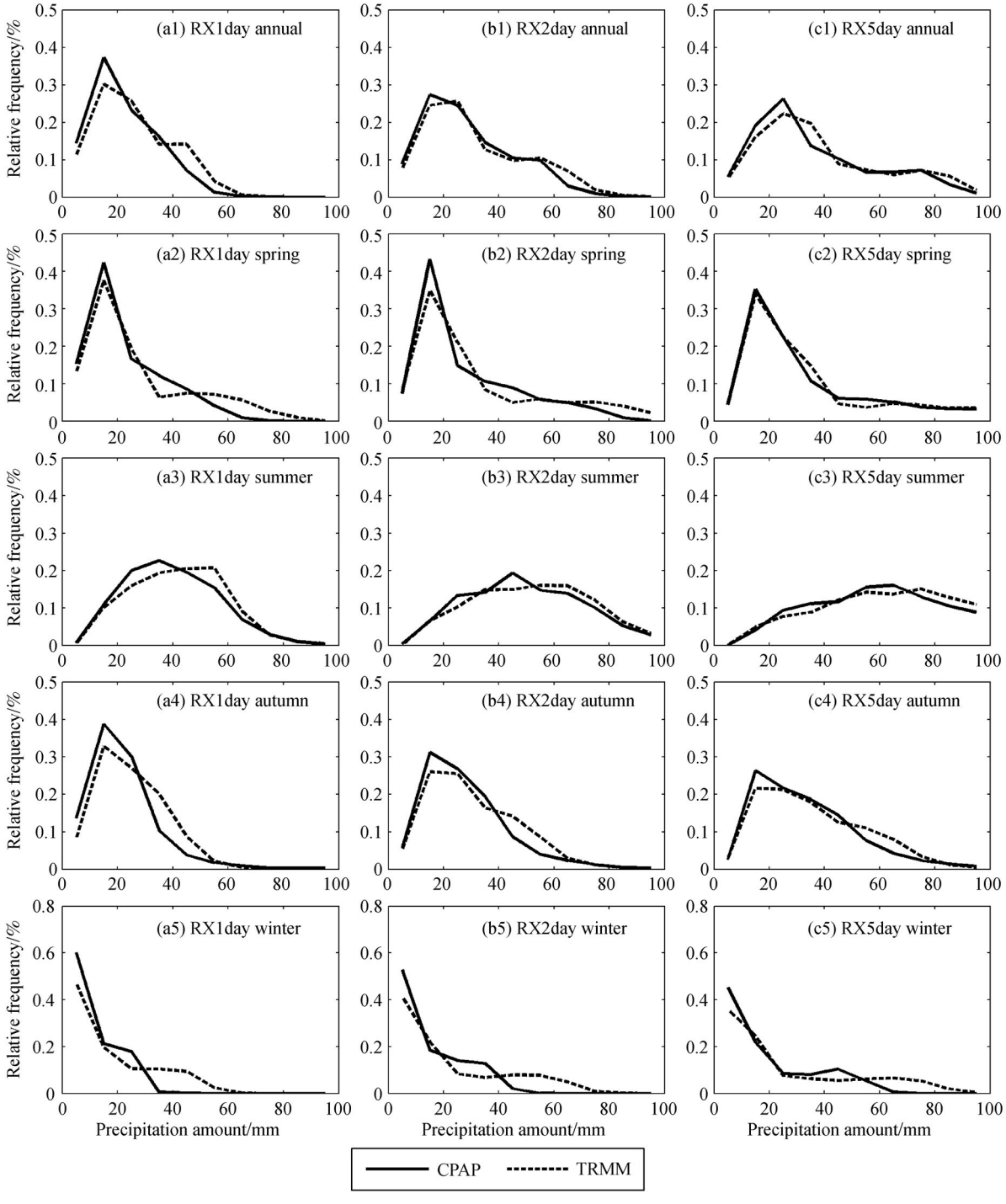

Fig. 2 The same as the Fig. 1 except for eastern China.

CPAP compared with the RX1day frequency. These findings are similar to those across China.

Figure 3 shows the comparison between the relative frequencies of RX1day, RX2day, and RX5day derived from TRMM 3B42-V7 and those derived from CPAP in western China. The agreement between the TRMM-based frequency and the CPAP-based frequency does not improve when the temporal scale increases from 1 day to 5 days, which is different from the TRMM 3B42-V7 performance over eastern China. Another difference between western China and eastern China is that TRMM 3B42-V7 performs differently for different seasons. The frequency is captured by TRMM 3B42-V7 well in winter, whereas disagreement between TRMM 3B42-V7 and CPAP is evident in the other three seasons. TRMM 3B42-V7 prominently underestimates the frequency for the ~20–40 mm precipitation amount range.

The performance of TRMM 3B42-V7 in reproducing frequencies of SDII, PRCPTOT, and R1 is shown in Fig. 4. For SDII, TRMM 3B42-V7 underestimates the frequency when SDII is below 18 mm/day but overestimates the frequency with SDII larger than 18 mm/day in eastern China, which is different from the results in western China where overestimation occurs with SDII smaller than 5 mm/day and underestimation occurs with SDII larger than 5 mm/day. RPCPTOT is well reproduced by TRMM 3B42-V7 in both eastern and western China. Unlike SDII, the shorter R1 is overestimated and the longer R1 is underestimated by TRMM 3B42-V7 in both eastern and western China.

Figure 5 shows the frequencies of CDD and CWD derived from CPAP and TRMM 3B42-V7. The frequency of shorter CDD is underestimated and the frequency of longer CDD is overestimated by TRMM 3B42-V7 in eastern China, whereas the frequency of shorter CDD is overestimated and the frequency of longer CDD is underestimation in western China. On the contrary, TRMM 3B42-V7 overestimates the frequency of shorter CWD and underestimate the frequency of longer CWD in eastern China. The performance in capturing CWD in western China is somewhat more complex. Slight frequency underestimation is found with shorter CWD, and overestimation with medium values, and underestimation with longer values.

4.3 Time series

The monthly time series analysis is conducted for RX1day, RX2day, and RX5day at both regional and grid cell scales. Generally, TRMM 3B42-V7 resembles the time series of monthly indices reasonably well, as shown in Fig. 6. The temporal correlation coefficients for RX1day, RX2day, and RX5day over the whole of China are 0.95, 0.96, and 0.98, respectively. The exact same values are found in eastern China. In contrast, the temporal correlation coefficients over western China are not as high as those over eastern China. The peak and valley time is not captured very well by TRMM 3B42-V7.

To evaluate the performance of TRMM 3B42-V7 in producing precipitation extremes at a single grid cell, we selected seven grid cells. Their centers in longitude–latitude are 116.375°E–39.875 °N, 87.625°E–43.875°N, 123.375°E–41.875°N, 114.375°E–30.625°N, 106.625°E–29.625°N, 121.375°E–31.125°N, and 113.375°E–23.125°N. These seven grid cells are close to the cities of Beijing, Urumchi, Shenyang, Wuhan, Chongqing, Shanghai, and Guangzhou, respectively, which are located in seven geophysical regions, namely, north, northwest, northeast, central, southwest, east, and southeast China, respectively. We name these grid cells by cities in the following analysis.

The performance of TRMM 3B42-V7 in producing RX1day, RX2day, and RX5day varies with geographic location, as shown in Fig. 7. At the Beijing grid cell (Fig. 7 (a1)–(c1)), TRMM 3B42-V7 produces the monthly maximum precipitation amount well at all temporal scales. The 23 July 2012 storm in Beijing is well captured by TRMM 3B42-V7. At the Urumchi grid cell (Fig. 7 (a2)–(c2)), TRMM 3B42-V7 significantly underestimates the maximum precipitation amount. The monthly maximum precipitation amount at Urumchi does not vary much with the temporal scale, because heavy rain does not usually last more than 1 day. At the Shenyang grid cell (Fig. 7(a3)–(c3)), the maximum precipitation amount is simulated reasonably well by TRMM 3B42-V7. However, the precipitation amount in summer 2011 is dramatically overestimated. At the Wuhan grid cell (Fig. 7(a4)–(c4)), underestimation and overestimation are mixed. At the Chongqing grid cell (Fig. 7(a5)–(c5)), a dramatic underestimation is found in summer 2009 and an overestimation in summer 2012. At the Shanghai grid cell (Fig. 7(a6)–(c6)), the TRMM 3B42-V7 does not perform well in producing the maximum precipitation amount. In August 2011, the monthly maximum precipitation derived from TRMM 3B42-V7 is several times larger than the CPAP-based maximum precipitation. At the Guangzhou grid cell (Fig. 7(a7)–(c7)), the large bias in summer is prominent.

5 Summary and discussion

In this study, we evaluated the TRMM 3B42-V7 product in capturing precipitation extreme over China. CPAP Version 1.0, developed by the National Meteorological Information Center of the China Meteorological Administration, was used as reference. Eight extreme indices, namely, monthly maximum 1-day precipitation (RX1day), monthly maximum consecutive 2-day precipitation (RX2day), monthly maximum 5-day consecutive precipitation (RX5day), simple daily intensity index (SDII), annual total precipitation amount for the wet days (PRCPTOT), annual wet days (R1), consecutive dry days (CDD), and consecutive wet

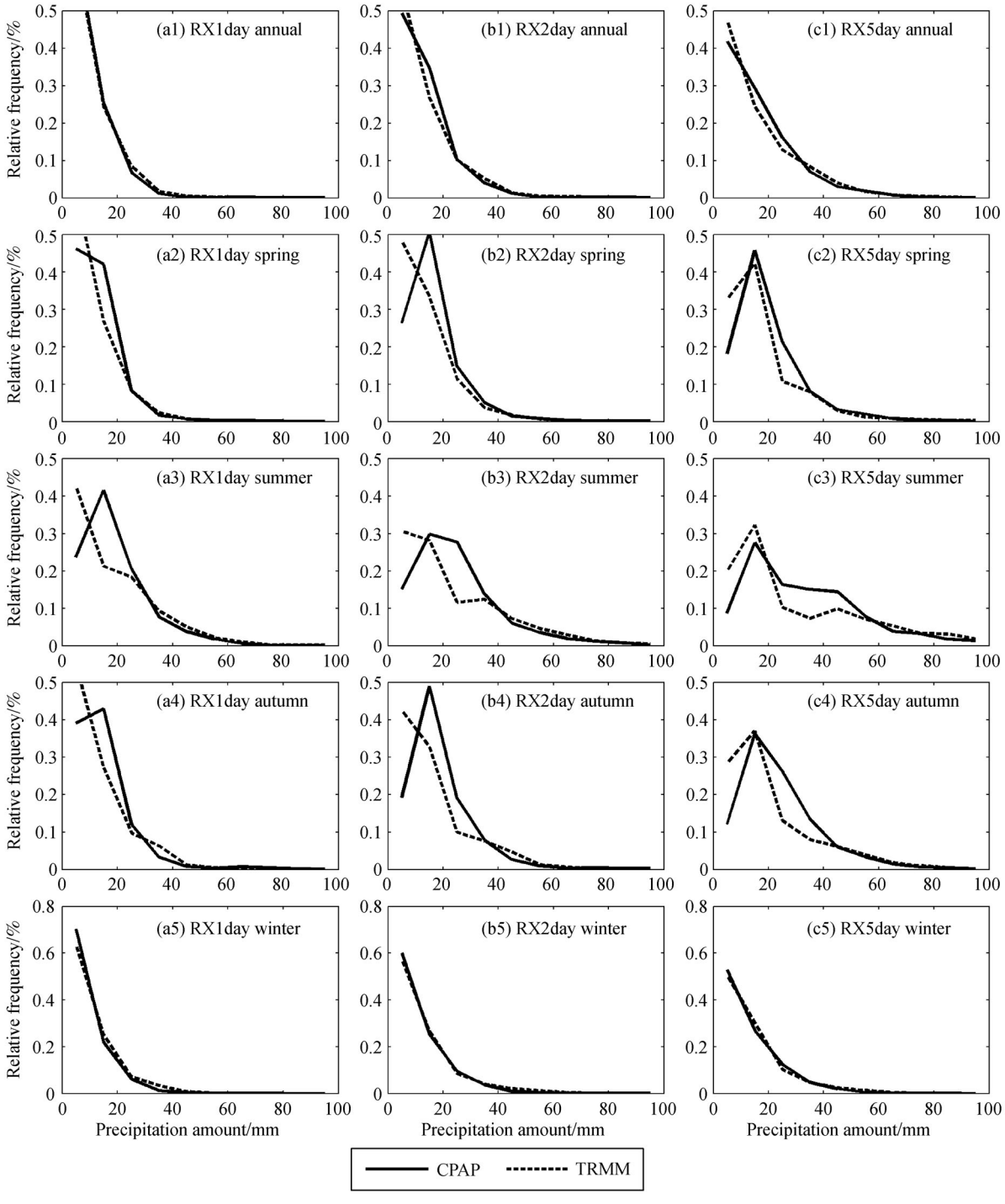

Fig. 3 The same as the Fig. 1 except for western China.

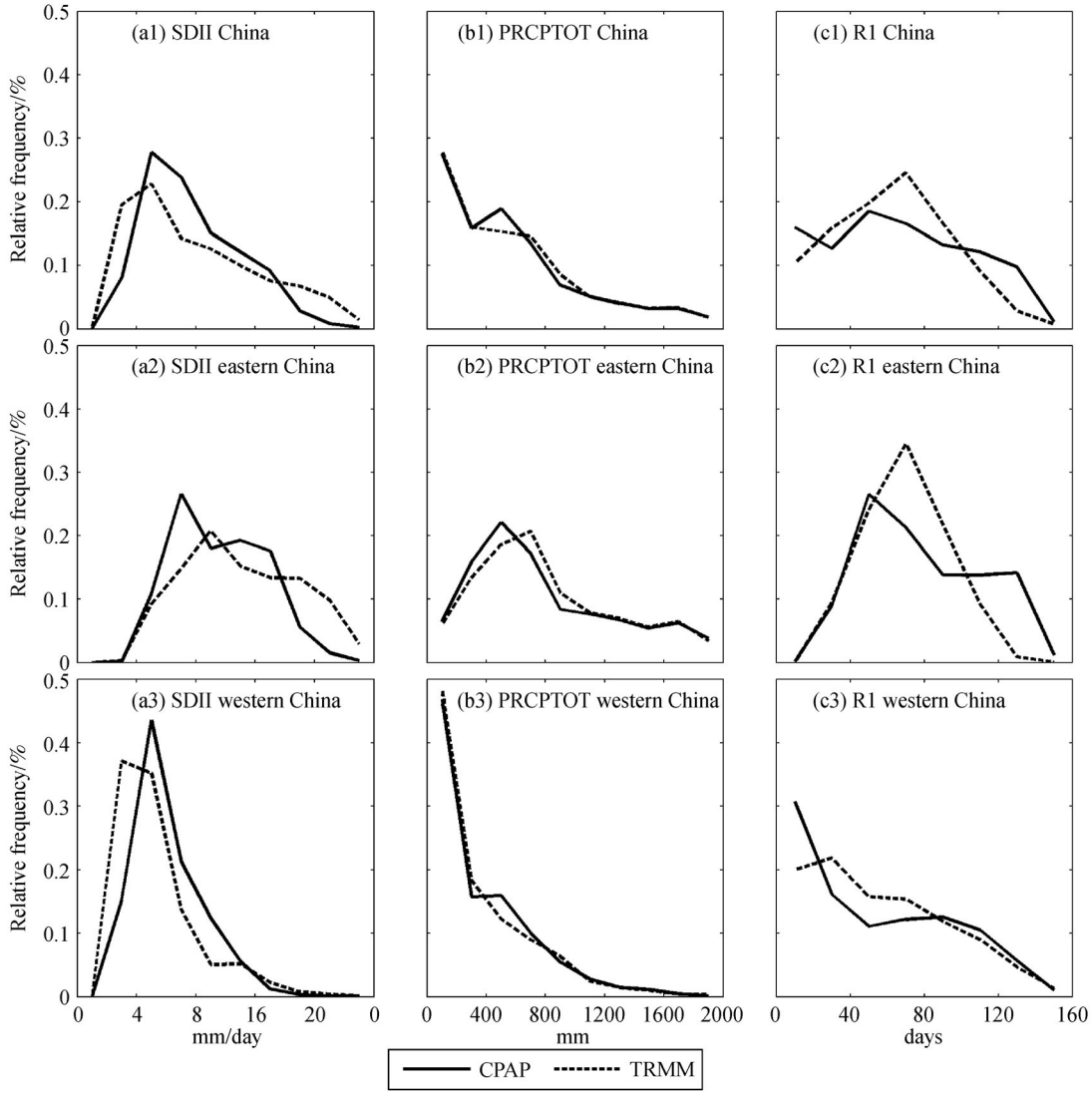

Fig. 4 The relative frequency of (a) SDII, (b) PRCPTOT, and (c) R1 derived from CPAP and TRMM 3B42-V7 over 1) China, 2) eastern China, and 3) western China.

days (CWD), were chosen to represent precipitation extreme characteristics. Assessments of the indices RX1day, RX2day, and RX5day were conducted annually, seasonally, and monthly, whereas evaluations of the indices SDII, PRCPTOT, R1, CDD, and CWD were carried out annually only.

The indices on the precipitation amount (RX1day, RX2day, RX5day, and PRCPTOT) derived from TRMM 3B42-V7 are in reasonable agreement with those based on gauge observations. Over China, MRB, NRMSE, and CC for PRCPTOT are –0.2%, 0.31, and 0.94, respectively. The satellite data performance in producing the monthly maximum precipitation amount improves when the temporal scale increases. For example, MRB reduces from 10.28% for RX1day to 3.19% for RX5day over China. However, the intensity and duration are not simulated very well by the satellite data. The CC values for SDII, R1, CDD, and CWD over China are 0.82, 0.84, 0.68, and 0.57, respectively, which are substantially smaller than the CC values for PRCPTOT, RX1day, RX2day, and RX5day.

The performance of the said satellite product varies with region. Generally, the satellite data are better over eastern China than over western China. Given that most of western China is composed of arid and semi-arid areas, possible reasons for the previous finding are as follows (Chen et al., 2013b): 1) hydrometeors detected by satellite sensors evaporate more quickly before falling to the ground in arid areas; 2) SSM/I-type sensors have difficulty in detecting precipitation over the desert because of the effect of land cover on the upwelling microwave radiation; 3) gauge stations are relatively sparse in western China, which causes the optimal interpolation scheme to distribute nonzero precipitation into zero precipitation areas. All

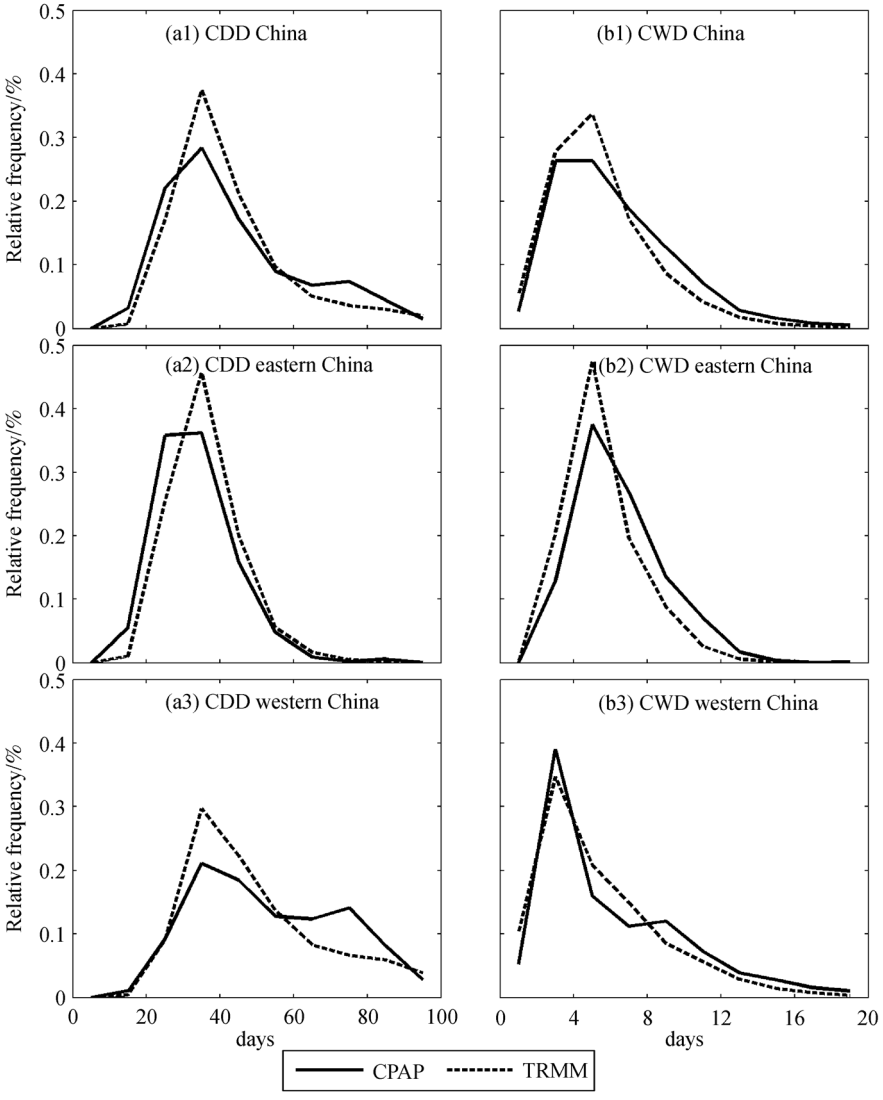

Fig. 5 The relative frequency of (a) CDD, and (b) CWD derived from CPAP and TRMM 3B42-V7 over 1) China, 2) eastern China, and 3) western China.

these factors lead to the inaccuracy of TRMM 3B42-V7 in western China. However, the MRB values are sometimes better over western China because of the offset between positive and negative biases. In producing RX1day, RX2day, and RX5day, TRMM 3B42-V7 performs differently for different seasons. Generally speaking, TRMM 3B42-V7 works best in summer and worst in winter among the four seasons. The large bias in winter is probably caused by the frozen land surface and ice particles in the air. Some high-frequency channels of PMW sensors might detect more scattering in such an environment, thereby seriously contaminating the retrievals (Vila et al., 2007).

PDFs derived from CPAP and TRMM 3B42-V7 are also examined for the eight indices. For RX1day, RX2day, and RX5day, overestimation in frequency with low and high precipitation amounts, together with underestimation in frequency with medium precipitation amounts, leads to a positive bias of TRMM 3B42-V7 in eastern China. The negative bias for RX1day, RX2day, and RX5day in western China results from the overestimation in frequency with low precipitation amounts and underestimation in frequency with medium precipitation amounts. Compared with TRMM-based frequencies of RX1day, RX2day, RX5day, and PRCPTOT, those of SDII, R1, CDD, and CWD do not agree well with their corresponding CPAP-based frequencies. The time series analysis for RX1day, RX2day, and RX5day shows that TRMM 3B42-V7 can produce the indices well at the large spatial scale. However, the performance of TRMM 3B42-V7 varies greatly with geographic locations at the grid cell scale.

Flood or drought monitoring is important because extreme events exert a damaging effect on human lives. Use of Satellite precipitation products provide an alternative method. This study indicates that TRMM 3B42-V7

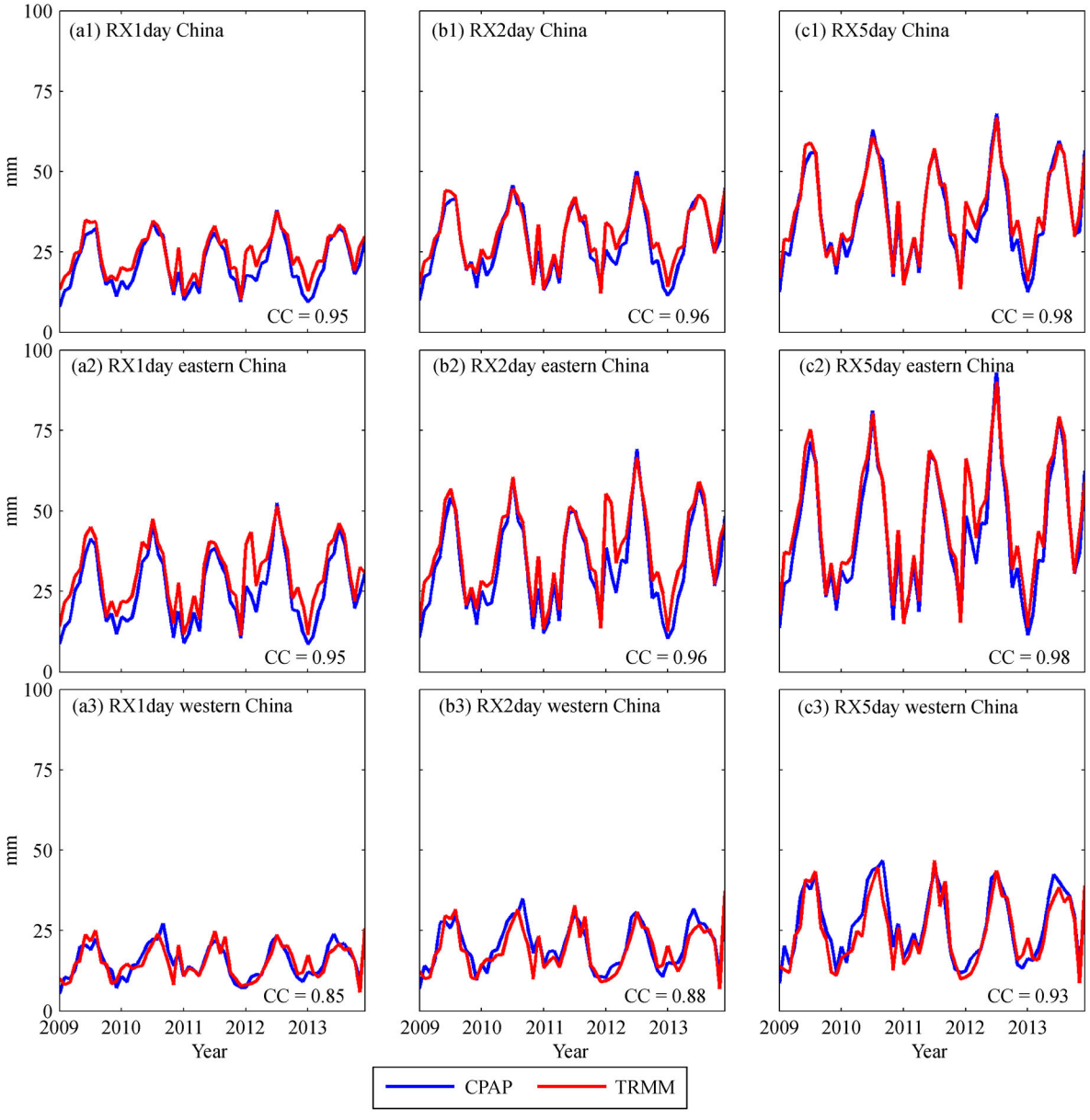

Fig. 6 The monthly values of indices of (a) RX1day, (b) RX2day, and (c) RX5day over 1) China, 2) Eastern China, 3) Western China derived from CPAP and TRMM 3B42-V7.

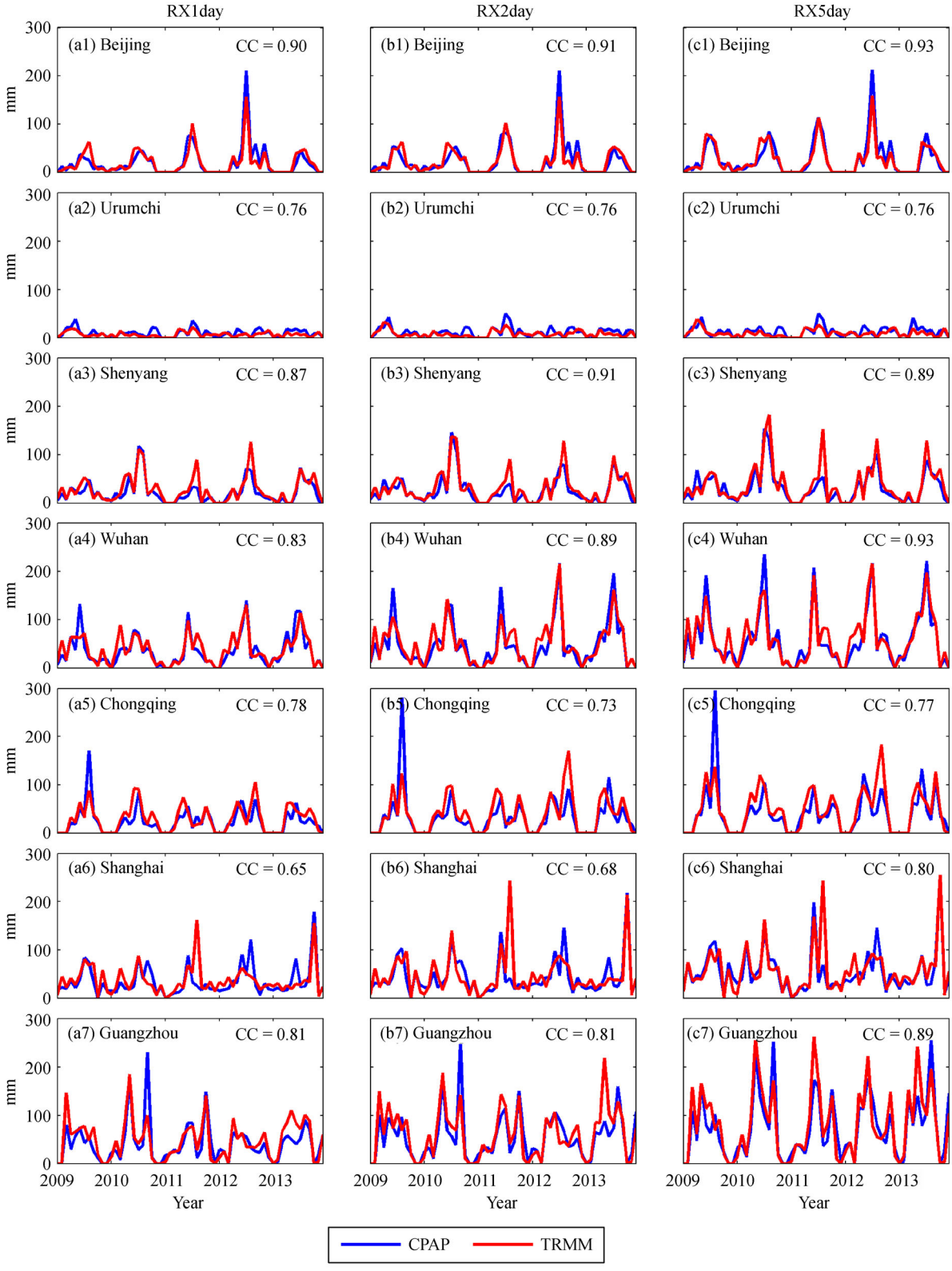

Fig. 7 The monthly values of indices of (a) RX1day, (b) RX2day, and (c) RX5day at a grid cell close to 1) Beijing, 2) Urumchi, 3) Shenyang, 4) Wuhan, 5) Chongqing, 6) Shanghai, and 7) Guangzhou derived from CPAP and TRMM 3B42-V7.

can realistically capture extreme precipitation amounts, especially at a large spatial scale. However, caution needs to be taken when using the satellite-based extreme indices for intensity and duration.

Acknowledgements This study is supported by the National Natural Science Foundation of China (Grant No. 51379224), the Fundamental Research Funds for the Central Universities (No. 15lgjc), and the Water Science and Technology Innovative Project of Guangdong Province (No. 2014-11).

References

AghaKouchak A, Behrangi A, Sorooshian S, Hsu K, Amitai E (2011). Evaluation of satellite-retrieved extreme precipitation rates across the central United States. J Geophys Res Atmos (1984–2012), 116(D2), doi: 10.1029/2010JD014741

Alexander L V, Zhang X, Peterson T C, Caesar J, Gleason B, Klein Tank A M G, Haylock M, Collins D, Trewin B, Rahimzadeh F, Tagipour A, Rupa Kumar K, Revadekar J, Griffiths G, Vincent L, Stephenson D B, Burn J, Aguilar E, Brunet M, Taylor M, New M, Zhai P, Rusticucci M, Vazquez-Aguirre J L (2013). Global observed changes in daily climate extremes of temperature and precipitation. J Geophys Res Atmos, 111: D05109

Allen C D, Macalady A K, Chenchouni H, Bachelet D, McDowell N, Vennetier M, Kitzberger T, Rigling A, Breshears D D, Hogg E H T, Gonzalez P, Fensham R, Zhang Z, Castro J, Demidova N, Lim J H, Allard G, Running S W, Semerci A, Cobb N (2010). A global overview of drought and heat-induced tree mortality reveals emerging climate change risks for forests. For Ecol Manage, 259 (4): 660–684

Asante K O, Macuacua R D, Artan G A, Lietzow R W, Verdin J P (2007). Developing a flood monitoring system from remotely sensed data for the Limpopo Basin. IEEE Trans Geosci Remote Sens, 45(6): 1709–1714

Chen S, Hong Y, Gourley J J, Huffman G J, Tian Y, Cao Q, Kirstetter P E, Hu J, Hardy J, Xue X (2013a). Evaluation of the successive V6 and V7 TRMM multi-satellite precipitation analysis over the continental United States. Water Resour Res, 10, doi: 10.1002/2012WR012795

Chen S, Hong Y, Gourley J J, Kirstette P E, Yong B, Tian Y, Zhang Z, Hardy J (2013b). Similarity and difference of the two successive V6 and V7 TRMM multi-satellite precipitation analysis (TMPA) performance over China. J Geophys Res, 118, doi: 10.1002/2013jd019964

Chen Y, Ebert E E, Walsh K J, Davidson N E (2013c). Evaluation of TMPA 3B42 daily precipitation estimates of tropical cyclone rainfall over Australia. J Geophys Res Atmos (1984–2012), 118(21): 11966–11978

De Boeck H J, Dreesen F E, Janssens I A, Nijs I (2011). Whole-system responses of experimental plant communities to climate extremes imposed in different seasons. New Phytol, 189(3): 806–817

Ebert E E, Janowiak J E, Kidd C (2007). Comparison of near-real-time precipitation estimates from satellite observations and numerical models. Bull Am Meteorol Soc, 88(1): 47–64

Hanson S, Nicholls R, Ranger N, Hallegatte S, Corfee-Morlot J, Herweijer C, Chateau J A (2011). Global ranking of port cities with high exposure to climate extremes. Clim Change, 104(1): 89–111

Hou A Y, Kakar R K, Neeck S, Azarbarzin A A, Kummerow C D, Kojima M, Oki R, Nakamura K, Iguchi T (2014). The global precipitation measurement mission. Bull Am Meteorol Soc, 95(5): 701–722

Huffman G J, Bolvin D T (2007). TRMM and other data precipitation data set documentation. Laboratory for Atmospheres, NASA Goddard Space Flight Center and Science Systems and Applications, Available online ftp://meso-a.gsfc.nasa.gov/pub/trmmdocs/3B42_3B43_doc.pdf

Huffman G J, Bolvin D T (2013). Real-Time TRMM Multi-Satellite Precipitation Analysis Data Set Documentation. ftp://meso-a.gsfc.nasa.gov/pub/trmmdocs/rt/ 3B4XRT_doc_V7.pdf

Huffman G J, Bolvin D T, Braithwaite D, Hsu K, Joyce R, Xie P (2014). GPM Integrated Multi-Satellite Retrievals for GPM (IMERG) Algorithm Theoretical Basis Document (ATBD) Version 4.4. PPS, NASA/GSFC, 30 pp. < http:// pmm.nasa.gov/sites/default/files/document_files/IMERG_ATBD_V4.4.pdf >

Huffman G J, Bolvin D T, Nelkin E J, Wolff D B, Adler R F, Gu G, Hong Y, Bowman K P, Stocker E F (2007). The TRMM multisatellite precipitation analysis (TMPA): quasi-global, multiyear, combined-sensor precipitation estimates at fine scales. J Hydrometeorol, 8(1): 38–55

Joyce R J, Janowiak J E, Arkin P A, Xie P (2004). CMORPH: a method that produces global precipitation estimates from passive microwave and infrared data at high spatial and temporal resolution. J Hydrometeorol, 5(3): 487–503

Kidd C, Bauer P, Turk J, Huffman G J, Joyce R, Hsu K L, Braithwaite D (2012). Intercomparison of high-resolution precipitation products over northwest Europe. J Hydrometeorol, 13(1): 67–83

Klein Tank A M G, Wijngaard J B, Können G P, Böhm R, Demarée G, Gocheva A, Mileta M, Pashiardis S, Hejkrlik L, Kern-Hansen C, Heino R, Bessemoulin P, Müller-Westermeier G, Tzanakou M, Szalai S, Pálsdóttir T, Fitzgerald D, Rubin S, Capaldo M, Maugeri M, Leitass A, Bukantis A, Aberfeld R, van Engelen A F V, Forland E, Mietus M, Coelho F, Mares C, Razuvaev V, Nieplova E, Cegnar T, Antonio López J, Dahlström B, Moberg A, Kirchhofer W, Ceylan A, Pachaliuk O, Alexander L V, Petrovic P (2002). Daily dataset of 20th-century surface air temperature and precipitation series for the European Climate Assessment. Int J Climatol, 22(12): 1441–1453

Li N, Tang G, Zhao P, Hong Y, Gou Y, Yang K (2017). Statistical assessment and hydrological utility of the latest multi-satellite precipitation analysis IMERG in Ganjiang River basin. Atmos Res, 183: 212–223

Liu Z (2015). Comparison of precipitation estimates between Version 7 3-hourly TRMM Multi-Satellite Precipitation Analysis (TMPA) near-real-time and research products. Atmos Res, 153: 119–133

Lockhoff M, Zolina O, Simmer C, Schulz J (2014). Evaluation of satellite-retrieved extreme precipitation over Europe using Gauge Observations. J Clim, 27(2): 607–623

Menne M J, Durre I, Vose R S, Gleason B E, Houston T G (2012). An overview of the global historical climatology network-daily database. J Atmos Ocean Technol, 29(7): 897–910

Michaelides S, Levizzani V, Anagnostou E, Bauer P, Kasparis T, Lane J

E (2009). Precipitation: measurement, remote sensing, climatology and modeling. Atmos Res, 94(4): 512–533

Moberg A, Jones P D (2005). Trends in indices for extremes in daily temperature and precipitation in central and western Europe, 1901–99. Int J Climatol, 25(9): 1149–1171

Monier E, Gao X (2014). Climate change impacts on extreme events in the United States: an uncertainty analysis. Clim Change, 131(1): 67–81

Nastos P T, Kapsomenakis J, Douvis K C (2013). Analysis of precipitation extremes based on satellite and high-resolution gridded data set over Mediterranean basin. Atmos Res, 131: 46–59

Peterson T, Daan H, Jones P (1997). Initial selection of a GCOS surface network. Bull Am Meteorol Soc, 78(10): 2145–2152

Prakash S, Mitra A K, Pai D S, AghaKouchak A (2016). From TRMM to GPM: how well can heavy rainfall be detected from space? Adv Water Resour, doi:10.1016/j.advwatres.2015.11.008

Qiao L, Hong Y, Chen S, Zou C B, Gourley J J, Yong B (2014). Performance assessment of the successive Version 6 and Version 7 TMPA products over the climate-transitional zone in the southern Great Plains, USA. J Hydrol (Amst), 513: 446–456

Rhee J, Im J, Carbone G J (2010). Monitoring agricultural drought for arid and humid regions using multi-sensor remote sensing data. Remote Sens Environ, 114(12): 2875–2887

Romilly T G, Gebremichael M (2011). Evaluation of satellite rainfall estimates over Ethiopian river basins. Hydrol Earth Syst Sci, 15(5): 1505–1514

Shen Y, Feng M, Zhang H, Gao F (2010a). Interpolation methods of China daily precipitation data. J Appl Meteor Sci, 21(3): 279–281 (in Chinese)

Shen Y, Xiong A, Wang Y, Xie P (2010b). Performance of high-resolution satellite precipitation products over China. J Geophys Res (1984−2012), 115(D2), doi: 10.1029/2009JD012097

Su F, Hong Y, Lettenmaier D P (2008). Evaluation of TRMM Multisatellite Precipitation Analysis (TMPA) and its utility in hydrologic prediction in the La Plata Basin. J Hydrometeorol, 9(4): 622–640

Tang G, Ma Y, Long D, Zhong L, Hong Y (2016). Evaluation of GPM Day-1 IMERG and TMPA version-7 legacy products over mainland China at multiple spatiotemporal scales. J Hydrol (Amst), 533: 152–167

Thibeault J M, Seth A (2014). Changing climate extremes in the Northeast United States: observations and projections from CMIP5. Clim Change, 127(2): 273–287

Tian Y, Peters-Lidard C D, Eylander J B, Joyce R J, Huffman G J, Adler R F, Hsu K, Turk FJ, Garcia M, Zeng J (2009). Component analysis of errors in satellite-based precipitation estimates. J Geophys Res Atmos (1984–2012), 114(D24), doi: 10.1029/2009JD011949

Vila D, Ferraro R, Joyce R (2007). Evaluation and improvement of AMSU precipitation retrievals. J Geophys Res Atmos (1984–2012), 112(D20), doi: 10.1029/2007JD008617

Westra S, Alexander L V, Zwiers F W (2013). Global increasing trends in annual maximum daily precipitation. J Clim, 26(11): 3904–3918

WMO (2014). Atlas of Mortality and Economic Losses from Weather, Climate and Water Extremes 1970−2012. Accessed on http://reliefweb.int/sites/reliefweb.int/files/resources/2014.06.12-wmo1123_Atlas_120614.pdf

Yong B, Chen B, Gourley J J, Ren L, Hong Y, Chen X, Wang W, Chen S, Gong L (2014). Intercomparison of the Version-6 and Version-7 TMPA precipitation products over high and low latitudes basins with independent gauge networks: Is the newer version better in both real-time and post-real-time analysis for water resources and hydrologic extremes? J Hydrol (Amst), 508: 77–87

Yong B, Liu D, Gourley J J, Tian Y, Huffman G J, Ren L L, Hong Y (2015). Global view of real-time TRMM multi-satellite precipitation analysis: implication to its successor global precipitation measurement mission. Bull Amer Meteor Soc, doi: 10.1175/BAMS-D-14-00017.1

You Q, Kang S, Aguilar E, Pepin N, Flügel W A, Yan Y, Xu Y, Zhang Y, Huang J (2011). Changes in daily climate extremes in China and their connection to the large scale atmospheric circulation during 1961–2003. Clim Dyn, 36(11−12): 2399–2417

Zhao T, Yatagai A (2014). Evaluation of TRMM 3B42 product using a new gauge-based analysis of daily precipitation over China. Int J Climatol, 34(8): 2749–2762

Zulkafli Z, Buytaert W, Onof C, Manz B, Tarnavsky E, Lavado W, Guyot J L (2014). A comparative performance analysis of TRMM 3B42 (TMPA) versions 6 and 7 for hydrological applications over Andean–Amazon River basins. J Hydrometeorol, 15(2): 581–592